

TECHNICAL RESEARCH REPORT

Sampled-Data Modeling and Analysis of PWM DC-DC Converters Part I. Closed-Loop Circuits

by C.-C. Fang, E.H. Abed

T.R. 98-54



ISR develops, applies and teaches advanced methodologies of design and analysis to solve complex, hierarchical, heterogeneous and dynamic problems of engineering technology and systems for industry and government.

ISR is a permanent institute of the University of Maryland, within the Glenn L. Martin Institute of Technology/A. James Clark School of Engineering. It is a National Science Foundation Engineering Research Center.

Web site <http://www.isr.umd.edu>

Sampled-Data Modeling and Analysis of PWM DC-DC Converters

I. Closed-Loop Circuits

Chung-Chieh Fang and Eyad H. Abed
Department of Electrical Engineering
and the Institute for Systems Research
University of Maryland
College Park, MD 20742 USA

Abstract

General block diagram models are proposed for PWM DC-DC converters in continuous and discontinuous conduction modes with fixed switching frequency. Both current mode control and voltage mode control are addressed in these models. Based on these models, detailed nonlinear and linearized sampled-data dynamics are derived. Asymptotic orbital stability is analyzed. Audio-susceptibility and output impedance are derived. In this approach, discontinuous conduction mode and current mode control can be analyzed systematically without special effort. A companion paper [1] addresses the same issues for the power stage of a PWM DC-DC converter.

1 Introduction

A DC-DC converter consists of a power stage (plant) and a controller (compensated error amplifier), as shown in Fig. 1. The objective of DC-DC conversion is to convert a source voltage to a near-constant output voltage under disturbances at the source voltage and load.

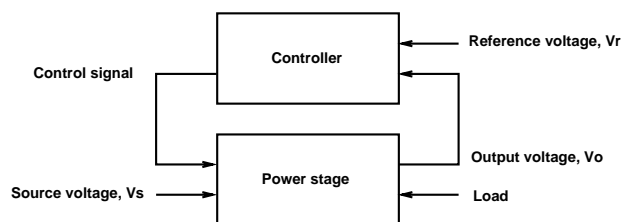


Figure 1: System diagram of a DC-DC converter

In this paper, PWM DC-DC converters are studied. The typical design approach of these converters is as follows. The power stage is modeled and analyzed by averaging methods [2, 3, 4]. Based on the averaged model, a controller is designed. Then simulation programs are used to test

the closed-loop performance.

There are some shortcomings in the approach just mentioned. The averaged models are approximate. The periodic solutions of PWM converters are averaged to equilibria. The averaged models do not accurately predict subharmonic instability [5], chaotic phenomena [6, 7, 8, 9], and steady-state DC offset [10]. Moreover, it has been found that the directly obtained averaged models are inaccurate for converters operated in discontinuous-conduction mode (DCM) or under current mode control. This has necessitated efforts to obtain more accurate averaged models for such cases [11, 12, 13, 14, 15, 16, 17, 18, 4]. Because of the nonlinear nature of PWM converters, a finite number of simulations does not necessarily reveal all possible behaviors of PWM converters.

The controlled switch plays a central role in the converter dynamics. It is therefore important to model the switch operation accurately. Since the switching action is essentially discrete, it is natural to consider the use of sampled-data modeling [19, 20, 21]. In [19], the ramp function which determines switching action is approximated by a constant threshold. In [20], a general approach is proposed without giving detailed modeling of PWM converters. Extensive numerical calculations are generally believed to be needed for sampled-data modeling. This has led many researchers to make approximations in their sampled-data models, such as using a straight line approximation for the system trajectory within a sampling period. Although such approximations can be useful if the switching frequency is sufficiently high, it has been shown in [22] that the resulting models can be inaccurate both qualitatively and quantitatively.

This paper extends previous works on sampled-data modeling for PWM converters with fixed switching frequency. General block diagram models for PWM DC-DC converters in continuous and discontinuous conduction modes are proposed. The ramp function, which is crucial in the dynamics, is carefully modeled. The models apply to current mode control and voltage mode control, as well as other possible control schemes. Based on the block diagram models, detailed nonlinear and linearized sampled-data sampled dynamics are derived. In this approach, discontinuous conduction mode and current mode control can be handled systematically, making the modeling for these cases simpler than with the use of averaging. Another important feature of this work is that the results

are exact if the source and reference voltage signals are constant. A companion paper [1] addresses the same issues for the power stage of a PWM DC-DC converter.

The performance of DC-DC converter is evaluated by steady-state analysis and dynamic analysis. In steady-state analysis, the existence and location of periodic solutions are of concern. In dynamic analysis, stability and transient dynamics can be studied using the closed-loop eigenvalues; line regulation and load regulation can be studied using audio-susceptibility and output impedance. Both steady-state and dynamic analysis will be done in the paper.

There exist many possible operating modes for the PWM converter because of its inherent nonlinear nature. Only two particular modes are of interests in practice: continuous conduction mode and discontinuous conduction mode. These two modes have 2 and 3 stages respectively in one cycle, and the dynamics is linear within each stage.

The organization of the paper is as follows. In Sec. 2, a general block diagram model for continuous conduction mode is proposed. By sampling the state, input and output at the same rate as the switching frequency, a nonlinear sampled-data model can be derived. The original periodic solution is a fixed point of the sampled-data model. Existence of fixed points is studied. Next, the linearized sampled-data dynamics near a fixed point is derived. Local orbital stability is then studied; audio-susceptibility and output impedance are derived. In Sec. 3, Similar steps are applied to discontinuous conduction mode. In Sec. 4, numerous illustrative examples are given. Conclusions are given in Sec. 5.

2 Continuous Conduction Mode (CCM)

2.1 Block Diagram Model

In this subsection, a block diagram model for the PWM converter in CCM is proposed. This model is shown to apply to current mode control and voltage mode control.

The proposed block diagram model for the PWM converter in CCM is shown in Fig. 2. In the diagram, $A_1, A_2 \in \mathbf{R}^{N \times N}$, $B_1, B_2 \in \mathbf{R}^{N \times 1}$, $C, E_1, E_2 \in \mathbf{R}^{1 \times N}$, and $D \in \mathbf{R}$ are constant matrices,

$x \in \mathbf{R}^N$, $y \in \mathbf{R}$ are the state (of power stage and controller) and the feedback signal, respectively. The source voltage is v_s ; the output voltage is v_o . The notation v_r denotes the reference signal, which could be a voltage or current reference. The reference signal v_r is allowed to be time-varying, although it is constant in most applications. The signal $h(t)$ is a T -periodic ramp. The clock has the same frequency $f_s = 1/T$ as the ramp. This frequency is called the switching frequency. The two stages in each clock period in CCM are denoted by S_1 and S_2 . The system is in S_1 immediately following a clock pulse, and switches to S_2 at instants $y(t) = h(t)$.

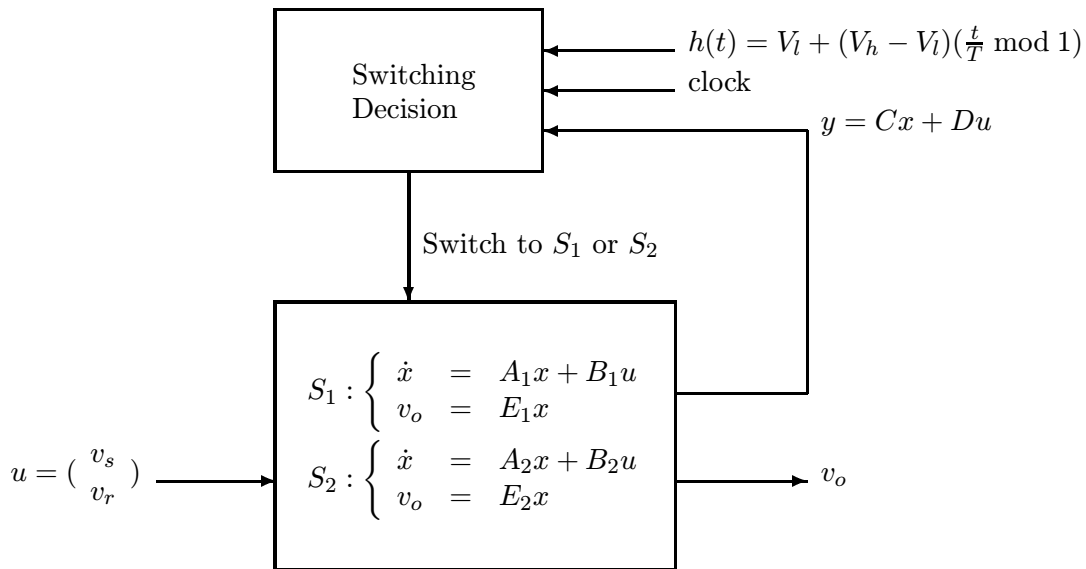


Figure 2: A block diagram model for PWM converters in CCM

Assume the switch and the diode in the PWM converter are ideal, so that there is no voltage drop when they are on. Most PWM converters can be modeled by Fig. 2. The PWM converter under current mode control fits this model exactly, with $h(t)$ denoting the slope-compensating ramp. For operation in voltage mode control, the system is switched between stages when the ramp signal $h(t)$ intersects with the feedback signal y . One of the switchings generally has the same frequency as the clock. Therefore the model in Fig. 2 is also good for the PWM converter under voltage mode control. Typical waveforms in current and voltage mode control are shown in Fig. 3 and Fig. 4, respectively. Many other control schemes (e.g., average current mode control) also fit the model in Fig. 2.

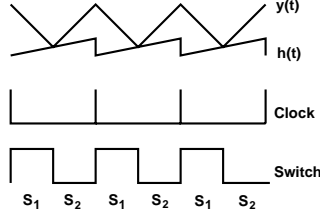


Figure 3: Waveforms of a PWM converter in CCM under current mode control

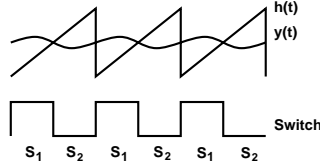


Figure 4: Waveforms of a PWM converter in CCM under voltage mode control

2.2 Nonlinear Sampled-Data Model

The switching action is essentially discrete. To arrive at a sampled-data model, the operation of the PWM converter within the $(n + 1)$ -st cycle, $t \in [nT, (n + 1)T)$, is considered. Generally in the PWM converter, the switching frequency is sufficiently high that the variations in v_s and v_r in a cycle can be neglected. Thus, take $u = (v_s, v_r)$ to be constant within the cycle, and denote its value by $u_n = (v_{sn}, v_{rn})$. Let $x_n = x(nT)$ and $v_{on} = v_o(nT)$. The sampled-data dynamics which maps x_n to x_{n+1} is derived next.

Denote by $nT + d_n$ the switching instant within the cycle when $y(t)$ and $h(t)$ intersect. Then $y(nT + d_n) = h(nT + d_n)$, and

$$S_1 : \begin{cases} \dot{x} &= A_1x + B_1u \\ v_o &= E_1x \end{cases} \quad \text{for } t \in [nT, nT + d_n) \quad (1)$$

$$S_2 : \begin{cases} \dot{x} &= A_2x + B_2u \\ v_o &= E_2x \end{cases} \quad \text{for } t \in [nT + d_n, (n + 1)T) \quad (2)$$

The two matrices E_1 and E_2 need not be the same. For example, they can differ if the equivalent series resistance (ESR) $R_c \neq 0$. When they differ, the output voltage is discontinuous. An example

of a discontinuous output voltage waveform is shown in Fig. 5. In most applications, the output voltage of interest is the maximum, minimum, or average voltage. So in the following, E is used to denote either E_1 , E_2 , or $(E_1 + E_2)/2$.

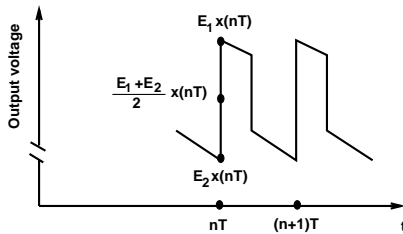


Figure 5: A discontinuous output voltage waveform

Using the dynamics (1) and (2) and the assumption that $u = (v_s, v_r)$ is constant within the cycle, one readily obtains the sampled-data dynamics (3)-(5) of the PWM converter in CCM. The dynamical equation (3) below is augmented with the constraint (4), corresponding to the intersection condition $y(nT + d_n) = h(nT + d_n)$ defining d_n .

$$\begin{aligned} x_{n+1} &= f(x_n, u_n, d_n) \\ &= e^{A_2(T-d_n)} \left(e^{A_1 d_n} x_n + \int_0^{d_n} e^{A_1(d_n-\sigma)} d\sigma B_1 u_n \right) + \int_{d_n}^T e^{A_2(T-\sigma)} d\sigma B_2 u_n \end{aligned} \quad (3)$$

$$\begin{aligned} g(x_n, u_n, d_n) &= y(nT + d_n) - h(nT + d_n) \\ &= C \left(e^{A_1 d_n} x_n + \int_0^{d_n} e^{A_1(d_n-\sigma)} d\sigma B_1 u_n \right) + D u_n - h(d_n) \\ &= 0 \end{aligned} \quad (4)$$

$$v_{on} = E x_n \quad (5)$$

2.3 Existence of T -Periodic Solutions

A T -periodic solution for system in Fig. 2 corresponds to a fixed point for the sampled-data model.

A periodic solution $x^0(t)$ is sampled as $x^0(0)$. Let the fixed point in the sampled-data dynamics

(3)-(5) be $(x_n, u_n, d_n) = (x^0(0), u, d)$, where $u = (V_s, V_r)'$. Then this fixed point satisfies

$$x^0(0) = f(x^0(0), u, d) \quad (6)$$

$$g(x^0(0), u, d) = 0 \quad (7)$$

where the functions $f(\cdot)$ and $g(\cdot)$ are given in Eqs. (3) and (4). These $N + 1$ nonlinear equations (Eqs. (6) and (7)) in $N + 1$ unknowns ($x^0(0)$ and d) can be solved by Newton's method [19]. After obtaining $x^0(0)$ and d , a periodic solution $x^0(t)$ is obtained:

$$x^0(t) = \begin{cases} e^{A_1 t} x^0(0) + \int_0^t e^{A_1(t-\sigma)} d\sigma B_1 u & \text{for } t \in [0, d) \\ e^{A_2(t-d)} x^0(d) + \int_d^t e^{A_2(t-\sigma)} d\sigma B_2 u & \text{for } t \in [d, T) \\ x^0(t \bmod T) & \text{for } t \geq T \end{cases} \quad (8)$$

A typical periodic solution $x^0(t)$ is shown Fig. 6.

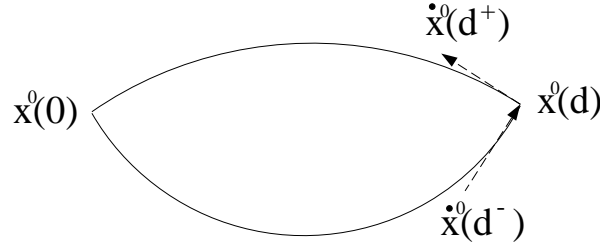


Figure 6: A typical periodic solution $x^0(t)$ of a PWM converter in state space

Next, consider the existence of fixed points in the sampled-data dynamics. Assume all of the eigenvalues of A_1 and A_2 are in the open left half of the complex plane, then the matrices $I - e^{A_2(T-d)} e^{A_1 d}$ and $I - e^{A_1 d} e^{A_2(T-d)}$ are invertible [23]. From Eq. (6), $x^0(0)$ can be expressed as

$$x^0(0) = (I - e^{A_2(T-d)} e^{A_1 d})^{-1} (e^{A_2(T-d)} \int_0^d e^{A_1(d-\sigma)} d\sigma B_1 u + \int_d^T e^{A_2(T-\sigma)} d\sigma B_2 u) \quad (9)$$

Similarly, $x^0(d)$ can be expressed as a function of d , denoted as $X_s(d)$:

$$X_s(d) = (I - e^{A_1 d} e^{A_2(T-d)})^{-1} (e^{A_1 d} \int_d^T e^{A_2(T-\sigma)} d\sigma B_2 u + \int_0^d e^{A_1(d-\sigma)} d\sigma B_1 u) \quad (10)$$

The function $X_s(\cdot)$ has the following property:

$$X_s(0) = -A_2^{-1}B_2u \quad (11)$$

$$X_s(T) = -A_1^{-1}B_1u \quad (12)$$

So the $N + 1$ equations, (6) and (7), reduce to one equation in one unknown d :

$$y(d) - h(d) = CX_s(d) + Du - h(d) = 0 \quad (13)$$

The next result gives a sufficient condition for existence of a fixed point in the sampled-data dynamics.

Theorem 1 *Assume that all of the eigenvalues of A_1 and A_2 are in the open left half of the complex plane. If*

$$(CA_2^{-1}B_2u - Du + h(0))(CA_1^{-1}B_1u - Du + h(T^-)) < 0 \quad (14)$$

then there exists a fixed point $(x_n, u_n, d_n) = (x^0(0), u, d)$ in the sampled-data dynamics (3)-(5).

Proof: From Eq. (13), if

$$\begin{aligned} & (CA_2^{-1}B_2u - Du + h(0))(CA_1^{-1}B_1u - Du + h(T^-)) \\ &= (CX_s(0) + Du - h(0))(CX_s(T) + Du - h(T^-)) \\ &< 0 \end{aligned}$$

then by the Intermediate Value Theorem, there exists a solution d satisfying Eq. (13). Hence there exists a fixed point $(x_n, u_n, d_n) = (x^0(0), u, d)$ in the sampled-data dynamics (3)-(5). \square

Note: Whenever there exists a T -periodic solution for the system in Fig. 2, it will be found as a fixed point in the sampled-data model. However, a fixed point in the the sampled-data model may not correspond to a T -periodic solution in Fig. 2. To explain the last remark, suppose a fixed point $(x_n, u_n, d_n) = (x^0(0), u, d)$ is obtained. Then a solution $x^0(t)$ can be obtained from Eq. (8). An example of signals $y^0(t) = Cx^0(t) + Du$ and $h(t)$ is shown in Fig. 7. The solution $y^0(t)$, although periodic with $y^0(d) = h(d)$, cannot be accepted because two switchings occur during $t \in (0, T)$.

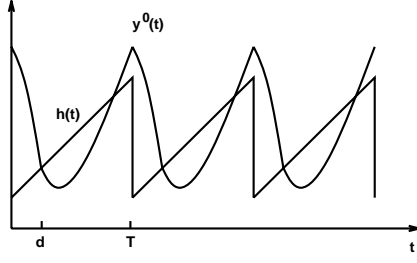


Figure 7: Ineligible signals $y^0(t)$ and $h(t)$ in voltage mode control

2.4 Linearized Sampled-Data Dynamics

The sampled-data dynamics (3)-(5) is constrained and nonlinear. Assuming that $\frac{\partial g}{\partial d_n} = C\dot{x}^0(d^-) - \dot{h}(d) \neq 0$, the Implicit Function Theorem allows one to linearize (3)-(5) at the fixed point $(x_n, u_n, d_n) = (x^0(0), u, d)$ to obtain an unconstrained linear sampled-data dynamical model. Using a hat $\hat{\cdot}$ to denote small perturbations (e.g., $\hat{x}_n = x_n - x^0(0)$), it follows that

$$\begin{aligned}\hat{x}_{n+1} &\approx \Phi \hat{x}_n + \Gamma \hat{u}_n \\ \hat{v}_{on} &= E \hat{x}_n\end{aligned}\tag{15}$$

where

$$\begin{aligned}\Phi &= \left. \frac{\partial f}{\partial x_n} - \frac{\partial f}{\partial d_n} \left(\frac{\partial g}{\partial d_n} \right)^{-1} \frac{\partial g}{\partial x_n} \right|_{(x_n, u_n, d_n) = (x^0(0), u, d)} \\ &= e^{A_2(T-d)} \left(I - \frac{((A_1 - A_2)x^0(d) + (B_1 - B_2)u)C}{C(A_1x^0(d) + B_1u) - \dot{h}(d)} \right) e^{A_1d} \\ &= e^{A_2(T-d)} \left(I - \frac{(\dot{x}^0(d^-) - \dot{x}^0(d^+))C}{C\dot{x}^0(d^-) - \dot{h}(d)} \right) e^{A_1d} \\ \Gamma &= \left. \frac{\partial f}{\partial u_n} - \frac{\partial f}{\partial d_n} \left(\frac{\partial g}{\partial d_n} \right)^{-1} \frac{\partial g}{\partial u_n} \right|_{(x_n, u_n, d_n) = (x^0(0), u, d)} \\ &= e^{A_2(T-d)} \left(\int_0^d e^{A_1\sigma} d\sigma B_1 - \frac{\dot{x}^0(d^-) - \dot{x}^0(d^+)}{C\dot{x}^0(d^-) - \dot{h}(d)} \left(C \int_0^d e^{A_1\sigma} d\sigma B_1 + D \right) \right) + \int_0^{T-d} e^{A_2\sigma} d\sigma B_2\end{aligned}\tag{16}$$

Recall that $u_n = (v_{sn}, v_{rn})'$, and denote $\Gamma = [\Gamma_1, \Gamma_2]$. Eq. (15) can be rewritten as

$$\begin{aligned}\hat{x}_{n+1} &\approx \Phi \hat{x}_n + \Gamma_1 \hat{v}_{sn} + \Gamma_2 \hat{v}_{rn} \\ \hat{v}_{on} &= E \hat{x}_n\end{aligned}\tag{18}$$

2.5 Stability Analysis

In the PWM converter, the steady-state operating condition is a *periodic solution*, not an equilibrium point as depicted in the averaging method. The relevant stability notion is *asymptotic orbital stability*. In the power electronics literature, the PWM converter is generally said to be either stable or unstable, without mentioning orbital stability per se. The definition of asymptotic orbital stability is given as follows.

Definition 1 (see, e.g., [24]) *Denote by γ the closed orbit generated by the periodic solution $x^0(t)$. Then $x^0(t)$ is asymptotically orbitally stable if there is a δ such that*

$$\text{dist}[x(0), \gamma] < \delta \Rightarrow \lim_{t \rightarrow \infty} \text{dist}[x(t), \gamma] = 0$$

where $\text{dist}[z, \gamma]$ is defined as the smallest distance between the point z and any point on γ .

Recall the following basic results on asymptotic orbital stability of the periodic solution $x^0(t)$.

Theorem 2 [24] *The fixed point $x^0(0)$ of the system (3)-(5) is asymptotically stable, or equivalently the periodic solution $x^0(t)$ in the original continuous-time system of Fig. 2 is asymptotically orbitally stable if all of the eigenvalues of Φ are inside the unit circle of the complex plane. Moreover, if $x^0(t)$ is asymptotically orbitally stable, then no eigenvalues of Φ lies outside the unit circle.*

The next result follows readily from the foregoing fact.

Theorem 3 *If the periodic solution $x^0(t)$ is asymptotically orbitally stable, then the following inequality holds:*

$$\left| \frac{C \dot{x}^0(d^+) - \dot{h}(d)}{C \dot{x}^0(d^-) - \dot{h}(d)} \right| \leq e^{\text{tr}[A_2 - A_1]d - \text{tr}[A_2]T}\tag{19}$$

Proof: Suppose the periodic solution $x^0(t)$ is asymptotically orbitally stable. Then all the eigenvalues of Φ have magnitude less than or equal than 1. Since $\det[\Phi]$ is the product of the eigenvalues of Φ , it follows that

$$\begin{aligned} |\det[\Phi]| &= \left| \det[e^{A_1 d} e^{A_2(T-d)}] \det\left[I - \frac{(\dot{x}^0(d^-) - \dot{x}^0(d^+))C}{C\dot{x}^0(d^-) - \dot{h}(d)}\right] \right| \\ &= e^{-\text{tr}[A_2 - A_1]d + \text{tr}[A_2]T} \left| \frac{C\dot{x}^0(d^+) - \dot{h}(d)}{C\dot{x}^0(d^-) - \dot{h}(d)} \right| \\ &\leq 1 \end{aligned}$$

The claim follows. □

Remark: Generally the switching period is so small that the right side of (19) can be approximated as 1, resulting in a condition that resembles a well-known stability criterion in current mode control [4, for example]:

$$\left| \frac{m_2 - m_c}{m_1 - m_c} \right| < 1 \quad (20)$$

where m_1 and $-m_2$ are the slopes of current trajectories during the on and off stages respectively using a *linear approximation* [2], and m_c is the slope of the compensating ramp. Theorem 3 differs from (20) in its use of instantaneous, rather than approximate, slope.

2.6 Comparison with Stability Analysis Using State-Space Averaging

The duty cycle changes from cycle to cycle. This variable determines when the switch is on or off, and it is crucial in the system dynamics. So this variable needs to be modeled properly. The averaging method, however, treats the duty cycle as a continuous-time variable.

Next, stability analysis using the averaging method is briefly summarized. For details, the reader is referred to [4]. Let the duty cycle in the averaging method be d_c , with nominal value D_c . Also let

$$A_{\text{ave}} = A_{\text{ON}}D_c + A_{\text{OFF}}(1 - D_c) \quad (21)$$

$$B_{\text{ave}} = B_{\text{ON}}D_c + B_{\text{OFF}}(1 - D_c) \quad (22)$$

$$E_{\text{ave}} = E_{\text{ON}}D_c + E_{\text{OFF}}(1 - D_c) \quad (23)$$

$$X_{\text{ave}} = -A_{\text{ave}}^{-1}B_{\text{ave}}V_s \quad (24)$$

The nominal solution by the averaging method is X_{ave} , a constant instead of a periodic solution $x^0(t)$. Linearized around the nominal operating point $(x, u, d_c) = (X_{\text{ave}}, (V_s, V_r)', D_c)$, the system in Fig. 2 has the following linearized *continuous-time* dynamics

$$\dot{\hat{x}} \approx A_{\text{ave}}\hat{x} + B_{\text{ave}}\hat{u} + ((A_{\text{ON}} - A_{\text{OFF}})X_{\text{ave}} + (B_{\text{ON}} - B_{\text{OFF}})u)\hat{d}_c \quad (25)$$

$$\hat{y} = C\hat{x} + D\hat{u} \quad (26)$$

$$\hat{v}_o = E_{\text{ave}}\hat{x} + (E_{\text{ON}} - E_{\text{OFF}})\hat{d}_c \quad (27)$$

with

$$\hat{d}_c = \begin{cases} \frac{\hat{y}}{V_h - V_l} = \frac{\hat{y}}{h(d)T} & \text{(for trailing-edge modulation, because } d_c = \frac{y - V_l}{V_h - V_l}) \\ \frac{-\hat{y}}{V_h - V_l} = \frac{-\hat{y}}{h(d)T} & \text{(for leading-edge modulation, because } d_c = \frac{V_h - y}{V_h - V_l}) \end{cases} \quad (28)$$

In either trailing-edge modulation (S_1 : switch on, S_2 : off) or leading-edge modulation (S_1 : off, S_2 : on), the closed-loop dynamics can be further simplified from Eqs. (25)-(28) to

$$\begin{aligned} \dot{\hat{x}} &\approx \mathcal{A}\hat{x} + \mathcal{B}\hat{u} \\ \hat{v}_o &= E_{\text{ave}}\hat{x} + (E_{\text{ON}} - E_{\text{OFF}})\hat{d}_c \end{aligned} \quad (29)$$

where (stage S_1 or S_2 can be either on or off stage)

$$\mathcal{A} = A_{\text{ave}} + ((A_1 - A_2)X_{\text{ave}} + (B_1 - B_2)u)\frac{C}{h(d)T} \quad (30)$$

$$\mathcal{B} = B_{\text{ave}} + ((A_1 - A_2)X_{\text{ave}} + (B_1 - B_2)u)\frac{D}{h(d)T} \quad (31)$$

The system is asymptotically stable if all of the eigenvalues of \mathcal{A} are in the open left half of the complex plane, which is equivalent to all of the eigenvalues of $\exp(\mathcal{A}T)$ being inside the unit circle. From Eq. (30), $\exp(\mathcal{A}T)$ can be written as

$$\exp(\mathcal{A}T) = e^{A_2(T-d) + A_1d + \frac{((A_1 - A_2)X_{\text{ave}} + (B_1 - B_2)u)C}{h(d)}} \quad (32)$$

which is similar in form to Φ in Eq. (16).

Comparing Eqs. (32) and (16), it is seen that the averaging method agrees with the sampled-data method under the following conditions:

1. $x^0(d)$ is approximated by X_{ave} (true if the periodic solution $x^0(t)$ is approximated by the equilibrium X_{ave}).
2. $C\dot{x}^0(d^-)$ is much smaller than $\dot{h}(d)$.
3. T is very small, so that $e^{(\dot{x}^0(d^-) - \dot{x}^0(d^+))CT} \approx I + (\dot{x}^0(d^-) - \dot{x}^0(d^+))CT$.
4. The matrices A_1 , A_2 and $(\dot{x}^0(d^-) - \dot{x}^0(d^+))C$ commute.

Note that condition 4 is unlikely to hold, and condition 2 generally does not hold for current mode control.

2.7 Audio-Susceptibility and Output Impedance

Audio-Susceptibility and output impedance are expressed in terms of transfer functions (frequency responses). They give information on the effect of disturbances at various frequencies on the output voltage.

The audio-susceptibility is derived directly from the linearized sampled-data model, Eq. (18).

It is

$$T_{os}(z) = \frac{\hat{v}_o(z)}{\hat{v}_s(z)} = E(zI - \Phi)^{-1}\Gamma_1 \quad (33)$$

To calculate the output impedance, add a fictitious current source i_o (as perturbation) in parallel with the load. Then the state equations in Eqs. (1) and (2) are replaced by

$$S_1 : \dot{x} = A_1x + B_{11}v_s + B_{12}v_r + B_{13}i_o \quad (34)$$

$$S_2 : \dot{x} = A_2x + B_{21}v_s + B_{22}v_r + B_{23}i_o \quad (35)$$

Since i_o is used as perturbation, the nominal value of i_o is 0. Similar to the derivation in Sec. 2.2, the new linearized sampled-data dynamics is

$$\begin{aligned} \hat{x}_{n+1} &\approx \Phi\hat{x}_n + \Gamma_1\hat{v}_{sn} + \Gamma_2\hat{v}_{rn} + \Gamma_3\hat{i}_{on} \\ \hat{v}_{on} &= E\hat{x}_n \end{aligned} \quad (36)$$

where

$$\begin{aligned}\Gamma_3 &= \frac{\partial f}{\partial i_{on}} - \frac{\partial f}{\partial d_n} \left(\frac{\partial g}{\partial d_n} \right)^{-1} \frac{\partial g}{\partial i_{on}} \Big|_{(x_n, u, d_n, i_{on})=(x^0(0), u, d, 0)} \\ &= e^{A_2(T-d)} \left(\int_0^d e^{A_1\sigma} d\sigma B_{13} - \frac{\dot{x}^0(d^-) - \dot{x}^0(d^+)}{C\dot{x}^0(d^-) - \dot{h}(d)} C \int_0^d e^{A_1\sigma} d\sigma B_{13} \right) \int_0^{T-d} e^{A_2\sigma} d\sigma B_{23}\end{aligned}\quad (37)$$

and i_{on} is the sampled perturbed output current. So the output impedance is

$$T_{oo}(z) = \frac{\hat{v}_o(z)}{\hat{i}_o(z)} = E(zI - \Phi)^{-1} \Gamma_3 \quad (38)$$

Given a transfer function in z domain, say $T(z)$, its effective frequency response [25, p. 93] is $T(e^{j\omega T})$, which is valid in the frequency range $|\omega| < \frac{\pi}{T}$.

3 Discontinuous Conduction Mode (DCM)

3.1 Block Diagram Model

There are three stages in DCM. The first two stages and their operation are the same as in CCM. The system is switched to the third stage when the inductor current i_L reaches zero. Within the third stage, $i_L = 0$. A block diagram model for the PWM converter in DCM is shown in Fig. 8. The matrix $F \in \mathbf{R}^{1 \times N}$ is chosen such that $Fx = i_L$. The remaining notation is the same as in Fig. 2.

3.2 Nonlinear Sampled-Data Model

Consider the operation of the PWM converter within the $(n + 1)$ -st cycle. As in CCM, take $u = (v_s, v_r)$ to be constant within the cycle and denote its value by $u_n = (v_{sn}, v_{rn})$.

Denote by $nT + d_{1n}$ the switching instant when $y(t)$ and $h(t)$ intersect within the cycle. (The notation d_{1n} , instead of $d_{1,n}$, is used for brevity.) Denote by $nT + d_{2n}$ the switching instant when the inductor current reaches zero. The three stages S_1, S_2, S_3 within the cycle are thus

$$S_1 : \begin{cases} \dot{x} &= A_1x + B_1u \\ v_o &= E_1x \end{cases} \quad \text{for } t \in [nT, nT + d_{1n}) \quad (39)$$

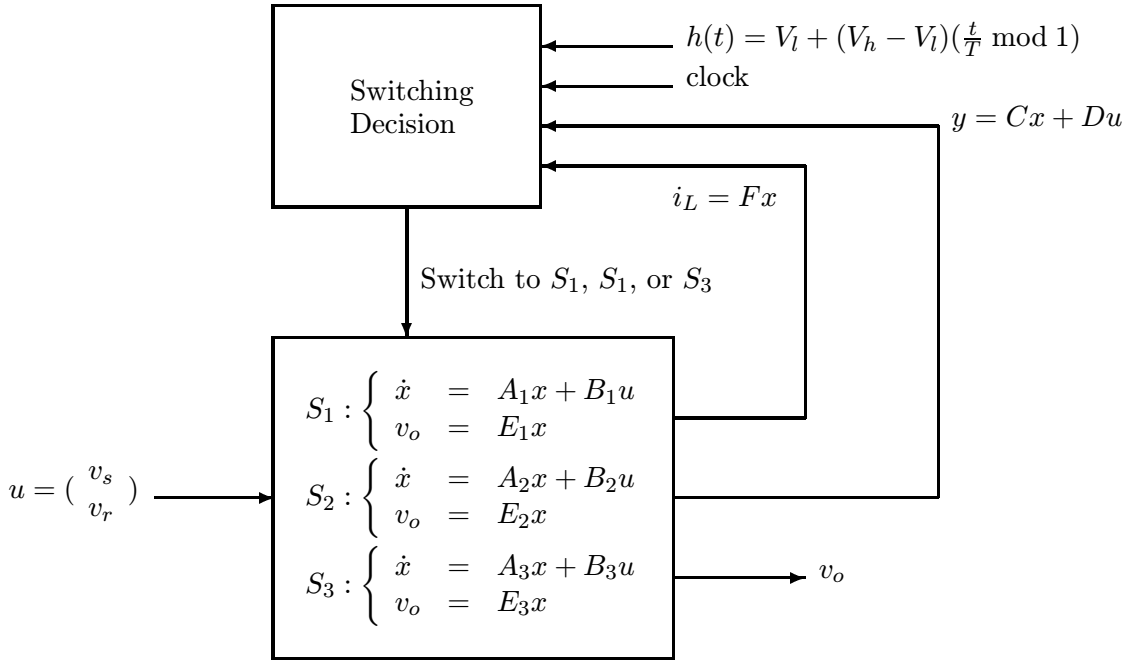


Figure 8: A block diagram model for PWM converters in DCM

$$S_2 : \begin{cases} \dot{x} = A_2x + B_2u \\ v_o = E_2x \end{cases} \quad \text{for } t \in [nT + d_{1n}, nT + d_{2n}) \quad (40)$$

$$S_3 : \begin{cases} \dot{x} = A_3x + B_3u \\ v_o = E_3x \end{cases} \quad \text{for } t \in [nT + d_{2n}, (n+1)T) \quad (41)$$

The two switching conditions are

$$Cx(nT + d_{1n}) + Du_n = h(nT + d_{1n}) \quad (42)$$

$$Fx(nT + d_{2n}) = 0 \quad (43)$$

As in CCM, the output voltage in DCM can be discontinuous at the clock time. Again, E is used to denote E_1 , E_3 , or $(E_1 + E_3)/2$ depending on which value of output voltage is of interest.

From Eqs. (39)-(43), the PWM converter in DCM has the following sampled-data dynamics:

$$\begin{aligned} x_{n+1} &= f(x_n, u_n, d_n) \\ &= e^{A_3(T-d_{2n})}(e^{A_2(d_{2n}-d_{1n})})(e^{A_1d_{1n}}x_n + \int_0^{d_{1n}} e^{A_1(d_{1n}-\sigma)}d\sigma B_1u_n) \end{aligned}$$

$$+ \int_{d_{1n}}^{d_{2n}} e^{A_2(d_{2n}-\sigma)} d\sigma B_2 u_n + \int_{d_{2n}}^T e^{A_3(T-\sigma)} d\sigma B_3 u_n \quad (44)$$

$$v_{on} = E x_n \quad (45)$$

$$\begin{aligned} g(x_n, u_n, d_n) &= \begin{bmatrix} Cx(nT + d_{1n}) + Du_n - h(nT + d_{1n}) \\ Fx(nT + d_{2n}) \end{bmatrix} \\ &= \begin{bmatrix} C(e^{A_1 d_{1n}} x_n + \int_0^{d_{1n}} e^{A_1 \sigma} d\sigma B_1 u_n) + Du_n - h(d_{1n}) \\ F(e^{A_2(d_{2n}-d_{1n})}(e^{A_1 d_{1n}} x_n + \int_0^{d_{1n}} e^{A_1 \sigma} d\sigma B_1 u_n) + \int_0^{d_{2n}-d_{1n}} e^{A_2 \sigma} d\sigma B_2 u_n) \end{bmatrix} \\ &= 0 \end{aligned} \quad (46)$$

where $d_n = (d_{1n}, d_{2n})'$. Since the inductor current always starts from 0 at the beginning of a cycle, another explicit constraint is $Fx_n = i_{Ln} = 0$, for *any* n . So the dynamics is $(N - 1)$ -dimensional instead of N -dimensional.

3.3 Linearized Sampled-Data Dynamics

Linearizing Eqs. (44)-(46) and using the notation \diamond to denote evaluation at the fixed point $(x_n, u_n, d_n) = (x^0(0), u, (d_1, d_2)')$, one has

$$\begin{aligned} \hat{x}_{n+1} &\approx \Phi \hat{x}_n + \Gamma \hat{u}_n \\ \hat{v}_{on} &= E \hat{x}_n \end{aligned} \quad (47)$$

where

$$\Phi = \left. \frac{\partial f}{\partial x_n} - \frac{\partial f}{\partial d_n} \left(\frac{\partial g}{\partial d_n} \right)^{-1} \frac{\partial g}{\partial x_n} \right|_{\diamond} \quad (48)$$

$$\Gamma = \left. \frac{\partial f}{\partial u_n} - \frac{\partial f}{\partial d_n} \left(\frac{\partial g}{\partial d_n} \right)^{-1} \frac{\partial g}{\partial u_n} \right|_{\diamond} \quad (49)$$

$$\left. \frac{\partial f}{\partial x_n} \right|_{\diamond} = e^{A_3(T-d_2)} e^{A_2(d_2-d_1)} e^{A_1 d_1} \quad (50)$$

$$\left. \frac{\partial f}{\partial d_n} \right|_{\diamond} = e^{A_3(T-d_2)} \begin{bmatrix} e^{A_2(d_2-d_1)} (\dot{x}^0(d_1^-) - \dot{x}^0(d_1^+)) & \dot{x}^0(d_2^-) - \dot{x}^0(d_2^+) \end{bmatrix} \quad (51)$$

$$\left. \frac{\partial g}{\partial d_n} \right|_{\diamond} = \begin{bmatrix} C\dot{x}^0(d_1^-) - \dot{h}(d_1) & 0 \\ F e^{A_2(d_2-d_1)} (\dot{x}^0(d_1^-) - \dot{x}^0(d_1^+)) & F\dot{x}^0(d_2^-) \end{bmatrix} \quad (52)$$

$$\left. \frac{\partial g}{\partial x_n} \right|_{\diamond} = \begin{bmatrix} C \\ F e^{A_2(d_2-d_1)} \end{bmatrix} e^{A_1 d_1} \quad (53)$$

$$\left. \frac{\partial f}{\partial u_n} \right|_{\diamond} = e^{A_3(T-d_2)} (e^{A_2(d_2-d_1)} \int_0^{d_1} e^{A_1 \sigma} d\sigma B_1 + \int_0^{d_2-d_1} e^{A_2 \sigma} d\sigma B_2) + \int_0^{T-d_2} e^{A_3 \sigma} d\sigma B_3 \quad (54)$$

$$\left. \frac{\partial g}{\partial u_n} \right|_{\diamond} = \begin{bmatrix} C \int_0^{d_1} e^{A_1 \sigma} d\sigma B_1 + D \\ F (e^{A_2(d_2-d_1)} \int_0^{d_1} e^{A_1 \sigma} d\sigma B_1 + \int_0^{d_2-d_1} e^{A_2 \sigma} d\sigma B_2) \end{bmatrix} \quad (55)$$

Since the inductor current i_L starts at 0 and ends at 0 in any cycle, it is not a dynamic variable. Thus, the dimension of the dynamics can be reduced by one. Note that this also implies that Φ possesses a zero eigenvalue, i.e. that $\det[\Phi] = 0$. This is shown in detail as follows:

$$\begin{aligned} \det[\Phi] &= \det[e^{A_3(T-d_2)} e^{A_2(d_2-d_1)} (I - \begin{bmatrix} \dot{x}^0(d_1^-) - \dot{x}^0(d_1^+) & e^{-A_2(d_2-d_1)} (\dot{x}^0(d_2^-) - \dot{x}^0(d_2^+)) \end{bmatrix})] \cdot \\ &\quad \left(\frac{\partial g}{\partial d_n} \right)^{-1} \Big|_{\diamond} \begin{bmatrix} C \\ F e^{A_2(d_2-d_1)} \end{bmatrix} e^{A_1 d_1} \\ &= \det[e^{A_1 d_1} e^{A_3(T-d_2)} e^{A_2(d_2-d_1)}] \det[I - \begin{bmatrix} C \\ F e^{A_2(d_2-d_1)} \end{bmatrix}] \cdot \\ &\quad \begin{bmatrix} \dot{x}^0(d_1^-) - \dot{x}^0(d_1^+) & e^{-A_2(d_2-d_1)} (\dot{x}^0(d_2^-) - \dot{x}^0(d_2^+)) \end{bmatrix} \left(\frac{\partial g}{\partial d_n} \right)^{-1} \Big|_{\diamond} \right] \\ &= \det[e^{A_1 d_1} e^{A_3(T-d_2)} e^{A_2(d_2-d_1)}] \cdot \\ &\quad \det[I - \begin{bmatrix} C(\dot{x}^0(d_1^-) - \dot{x}^0(d_1^+)) & C e^{-A_2(d_2-d_1)} (\dot{x}^0(d_2^-) - \dot{x}^0(d_2^+)) \\ F e^{A_2(d_2-d_1)} (\dot{x}^0(d_1^-) - \dot{x}^0(d_1^+)) & F \dot{x}^0(d_2^-) \end{bmatrix}] \cdot \\ &\quad \frac{\begin{bmatrix} F \dot{x}^0(d_2^-) & 0 \\ -F e^{A_2(d_2-d_1)} (\dot{x}^0(d_1^-) - \dot{x}^0(d_1^+)) & C \dot{x}^0(d_1^-) - \dot{h}(d_1) \end{bmatrix}}{(C \dot{x}^0(d_1^-) - \dot{h}(d_1)) F \dot{x}^0(d_2^-)} \\ &= \det[e^{A_1 d_1} e^{A_3(T-d_2)} e^{A_2(d_2-d_1)}] \det[I - \begin{bmatrix} * & * \\ 0 & 1 \end{bmatrix}] \\ &= 0 \end{aligned}$$

here * signifies an irrelevant term.

The stability, audio-susceptibility and output impedance analysis are similar to the case in CCM

and are omitted.

4 Illustrative Examples

Example 1 (*Local vs. global orbital stability*, [10, p. 90]) Consider the boost converter shown in Fig. 9, where $T = 2\mu s$, $V_s = 4V$, $L = 5.24\mu H$, $C = 0.2\mu F$, $R = 16\Omega$, $k_1 = -0.1$, $k_2 = 0.01$, $V_r = 0.48V$, and $h(t) = ((\frac{t}{T}) \bmod 1)$.

Although the control scheme is neither voltage nor current mode control, the circuit can still be expressed in terms of the block diagram model in Fig. 2, with state $x = (i_L, v_C)$:

$$\begin{aligned} A_1 &= \begin{bmatrix} 0 & 0 \\ 0 & \frac{-1}{RC} \end{bmatrix} & A_2 &= \begin{bmatrix} 0 & \frac{-1}{L} \\ \frac{1}{C} & \frac{-1}{RC} \end{bmatrix} & B_1 &= B_2 = \begin{bmatrix} \frac{1}{L} \\ 0 \end{bmatrix} \\ C &= \begin{bmatrix} -k_1 & -k_2 \end{bmatrix} & D &= \begin{bmatrix} 0 & 1 \end{bmatrix} & E_1 &= E_2 = \begin{bmatrix} 0 & 1 \end{bmatrix} \end{aligned}$$

The periodic solution calculated using Eq. (8) is shown in Fig. 10. The closed-loop poles calculated from Eq. (16) are $\sigma(\Phi) = 0.8 \pm 0.45i$, which are inside the unit circle. So the periodic solution is *locally* orbitally stable. The magnitude of the eigenvalues is 0.9225, indicating that the settling time to the steady state may be long. For example, let the initial state be $(i_L, v_C) = (0.9, 8)$. The simulated output voltage is shown in Fig. 11. After the transient, the state trajectory goes to the periodic solution.

The averaging method also predicts local stability. From Sec. 2.6, the closed-loop poles predicted by the averaging method are

$$\sigma(\mathcal{A}) = (-0.2759 \pm 2.9276i) \times 10^5 \quad (56)$$

and $e^{\sigma(\mathcal{A})T} = 0.7887 \pm 0.5230i$, close to the eigenvalues found above using by the sampled-data method.

However, the circuit is not globally stable and is described in [10] as being unstable based on simulation. Since the averaging method is for local (small-signal) analysis, it is not surprising that it cannot predict lack of global stability.

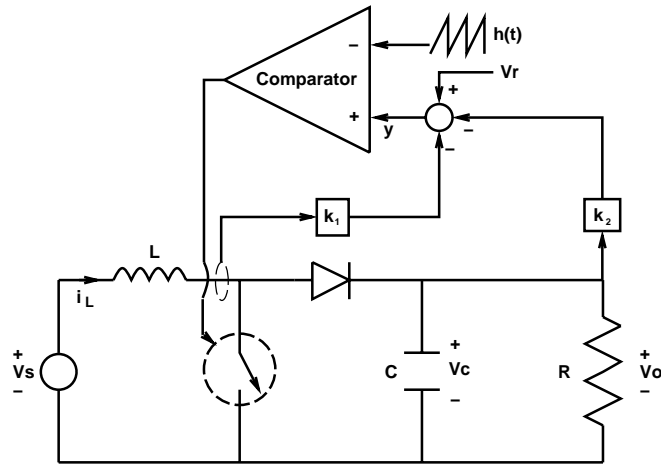


Figure 9: System diagram for Example 1

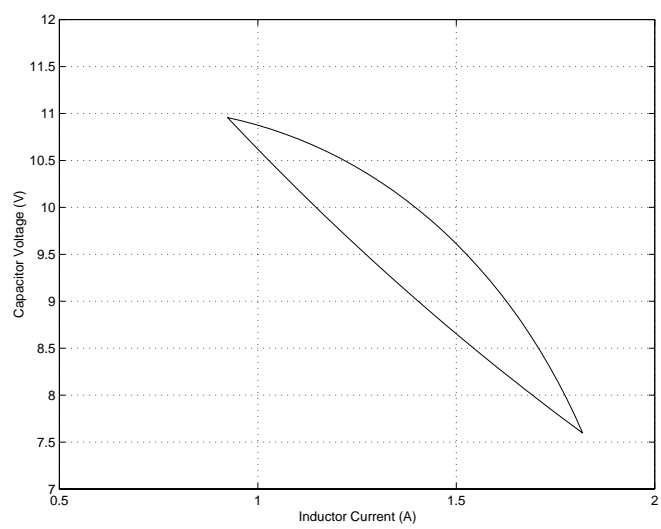


Figure 10: Periodic solution in Example 1

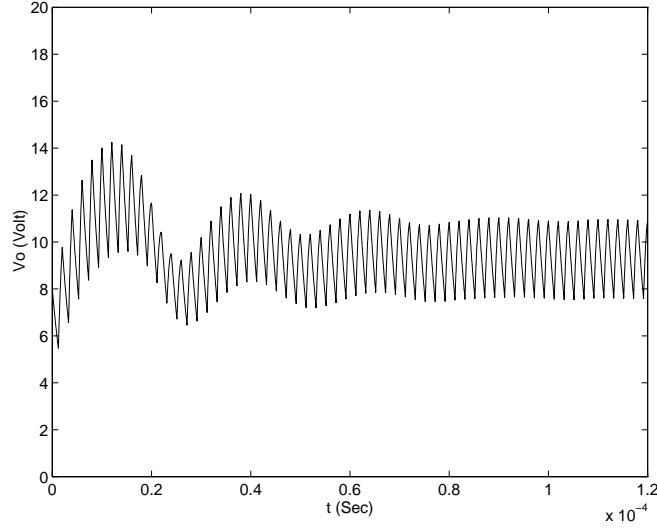


Figure 11: Output voltage trajectory in Example 1 for initial condition $(i_L, v_C) = (0.9, 8)$

Example 2 (*Buck converter under voltage mode phase-lead control*, [4, p. 346]) The system diagram is shown in Fig. 12. The system parameters are as follows: $T = 10\mu s$, $V_s = 28V$, $R = 3\Omega$, $L = 50\mu H$, $C = 500\mu F$, $V_r = 5V$, $G_{c0} = 3.7$, $\omega_z = 10681 \text{ rad/sec}$, $\omega_p = 91106 \text{ rad/sec}$, and $h(t) = 4(\frac{t}{T} \bmod 1)$. The voltage divider gain g_{vd} is chosen to be 0.29465 (instead of 1/3 in [4]) to result in an output voltage at 15V.

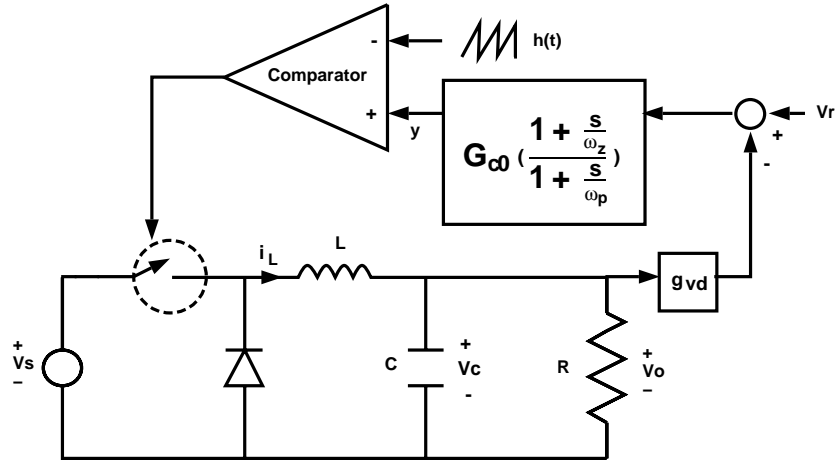


Figure 12: System diagram for Example 2

Let the state $x = (i_L, v_C, x_c)$, where x_c is the state of the error amplifier. In terms of the

representation in Fig. 2,

$$\begin{aligned}
A_1 &= A_2 = \begin{bmatrix} 0 & \frac{-1}{L} & 0 \\ \frac{1}{C} & \frac{-1}{RC} & 0 \\ 0 & g_{vd}(\omega_p - \omega_z) & -\omega_p \end{bmatrix} \\
B_1 &= \begin{bmatrix} \frac{1}{L} & 0 \\ 0 & 0 \\ 0 & \omega_z - \omega_p \end{bmatrix} & B_2 &= \begin{bmatrix} 0 & 0 \\ 0 & 0 \\ 0 & \omega_z - \omega_p \end{bmatrix} \\
C &= \frac{G_{c0}\omega_p}{\omega_z} \begin{bmatrix} 0 & -g_{vd} & 1 \end{bmatrix} & D &= \begin{bmatrix} 0 & \frac{G_{c0}\omega_p}{\omega_z} \end{bmatrix} \\
E_1 &= E_2 = \begin{bmatrix} 0 & 1 & 0 \end{bmatrix}
\end{aligned}$$

Solving Eqs. (9) and (13) by Newton's method results in $x^0(0) = (4.3, 15, -0.512)$ and $d = 5.36 \times 10^{-6}$. The eigenvalues of the closed-loop system can be obtained from $\sigma[\Phi]$ and they are 0.8096 ± 0.1154 and 0.5973 . So the periodic solution $x^0(t)$ is asymptotically orbitally stable.

Example 3 (*Boost converter under current mode control with voltage loop closed*, [26]) The system diagram is shown in Fig. 13, where $f_s = 25kHz$, $V_s = 28V$, $R = 11.2\Omega$, $L = 195\mu H$, $C = 2mF$, $R_1 = 47.5k\Omega$, $R_2 = 2.5k\Omega$, $R_s = 0.8125\Omega$, $R_f = 72.2\Omega$, and $C_f = 0.23\mu F$. The source voltage V_s and thus the duty cycle are varied. The system is analyzed for two situations: without slope compensation ($h(t) = 0$), and with slope compensation ($h(t) = (\frac{R_s V_s T}{5L})[\frac{t}{T} \bmod 1]$).

Let the state $x = (i_L, v_C, v_{cf})$. The system matrices in Fig. 3.1 are

$$\begin{aligned}
A_1 &= \begin{bmatrix} 0 & 0 & 0 \\ 0 & \frac{-1}{RC} & 0 \\ 0 & \frac{1}{C_f R_1} & 0 \end{bmatrix} & A_2 &= \begin{bmatrix} 0 & \frac{-1}{L} & 0 \\ \frac{1}{C} & \frac{-1}{RC} & 0 \\ 0 & \frac{-1}{C_f R_f} & 0 \end{bmatrix} \\
B_1 &= B_2 = \begin{bmatrix} \frac{1}{L} & 0 \\ 0 & 0 \\ 0 & \frac{1}{C_f R_1} + \frac{1}{C_f R_2} \end{bmatrix} & D &= \begin{bmatrix} 0 & 1 + \frac{R_f}{R_1} + \frac{R_f}{R_2} \end{bmatrix} \\
C &= \begin{bmatrix} -R_s & \frac{-R_f}{R_1} & 1 \end{bmatrix} & E_1 &= E_2 = \begin{bmatrix} 0 & 1 & 0 \end{bmatrix}
\end{aligned}$$

Consider the system without slope compensation. The duty cycle is varied from 0.4 to 0.6 and $\sigma[\Phi]$ is plotted and shown in Fig. 14. One eigenvalue trajectory crosses the unit circle at $D_c = 0.498$. The other two remain very close to 1. For $D_c > 0.498$, the system is unstable.

Next, consider the system with slope compensation. The duty cycle is varied from 0.4 to 0.7 and $\sigma[\Phi]$ is calculated. One eigenvalue trajectory crosses the unit circle at $D_c = 0.5845$. For

$D_c > 0.5845$, the system is unstable.

In [26], the system is reported to be unstable for $D_c > 0.454$ without slope compensation and for $D_c > 0.61$ with slope compensation.

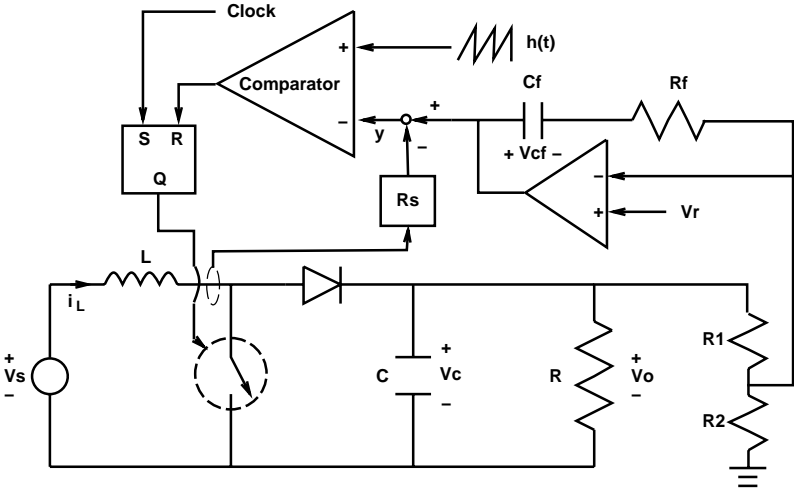


Figure 13: System diagram for Example 3

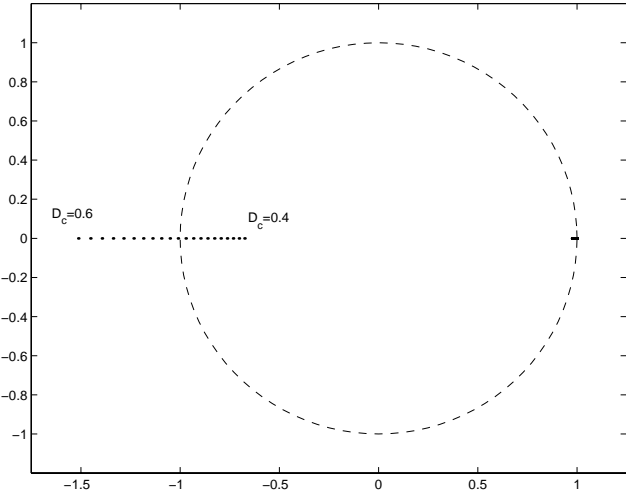


Figure 14: $\sigma(\Phi)$ as D_c varies from 0.4 to 0.6

5 Concluding Remarks

General block diagram models have been proposed for PWM DC-DC converters in continuous and discontinuous conduction modes with fixed switching frequency. Both current mode control and voltage mode control are addressed by these models. Based on the models, detailed nonlinear and linearized sampled-data dynamics have been derived. Asymptotic orbital stability has been analyzed, and audio-susceptibility and output impedance have been derived.

Compared with the averaging approach, the sampled-data approach has the following characteristics and advantages. An assumption in the sampled-data approach is that the source voltage and reference signal can be viewed as constant within each cycle. This assumption is reasonable because the switching frequency is generally very high. Once the circuit operations are understood, the derivation of the sampled-data dynamics in various modes and control schemes are straight forward and elegant. For example, discontinuous conduction mode and current mode control can be analyzed by this unified approach. Since fewer assumptions are made than in the averaging approach, the sampled-data approach is more accurate. The only numerical extensive procedure in the sampled-data approach is to find the fixed-point. The remaining analysis is eased by the analytical form of the dynamic models. The sampled-data approach should be applied to double check closed-loop performance whenever a PWM DC-DC converter is designed.

Some extensions of this paper and the companion paper [1] have been done in the first author's dissertation [23]. These extensions include modeling and analysis of load-resonant converters, and control designs of both PWM and load-resonant converters.

Acknowledgments

This research has been supported in part by the the Office of Naval Research under Multidisciplinary University Research Initiative (MURI) Grant N00014-96-1-1123, the U.S. Air Force Office of Scientific Research under Grant F49620-96-1-0161, and by a Senior Fulbright Scholar Award.

References

- [1] C.-C. Fang and E.H. Abed, "Sampled-data modeling and analysis of PWM DC-DC converters II. The power stage," preprint, Feb. 1998.

- [2] R.D. Middlebrook and S. Ćuk, “A general unified approach to modelling switching-converter power stages,” in *IEEE Power Electronics Specialists Conf. Rec.*, 1976, pp. 18–34.
- [3] S. Ćuk and R.D. Middlebrook, “A general unified approach to modelling switching DC-to-DC converters in discontinuous conduction mode,” in *IEEE Power Electronics Specialists Conf. Rec.*, 1977, pp. 36–57.
- [4] R.W. Erickson, *Fundamentals of Power Electronics*, Chapman and Hall, New York, 1997.
- [5] A.R. Brown and R.D. Middlebrook, “Sampled-data modelling of switching regulators,” in *IEEE Power Electronics Specialists Conf. Rec.*, 1981, pp. 349–369.
- [6] J.H.B. Deane and D.C. Hamill, “Instability, subharmonics, and chaos in power electronics circuits,” *IEEE Transactions on Power Electronics*, vol. 5, no. 3, pp. 260–268, 1990.
- [7] D.C. Hamill, J.H.B. Deane, and J. Jefferies, “Modeling of chaotic DC-DC converters by iterated nonlinear mappings,” *IEEE Transactions on Power Electronics*, vol. 7, no. 1, pp. 25–36, 1992.
- [8] J.H.B. Deane, “Chaos in a current-mode controlled boost DC-DC converter,” *IEEE Transactions on Circuits and Systems-I: Fundamental Theory and Applications*, vol. 39, no. 8, pp. 680–683, 1992.
- [9] C.K. Tse, “Flip bifurcation and chaos in three-state boost switching regulators,” *IEEE Transactions on Circuits and Systems-I: Fundamental Theory and Applications*, vol. 41, no. 1, pp. 16–23, 1994.
- [10] B. Lehman and R.M. Bass, “Switching frequency dependent averaged models for PWM DC-DC converters,” *IEEE Transactions on Power Electronics*, vol. 11, no. 1, pp. 89–98, 1996.
- [11] V. Vorperian, “Simplified analysis of PWM converters using model of PWM switch. II. Discontinuous conduction mode,” *IEEE Transactions on Aerospace and Electronic Systems*, vol. 26, no. 3, pp. 497–505, 1990.
- [12] D. Maksimovic and S. Cuk, “A unified analysis of PWM converters in discontinuous modes,” *IEEE Transactions on Power Electronics*, vol. 6, no. 3, pp. 476–490, 1991.
- [13] Shi-Ping Hsu, A. Brown, L. Rensink, and R.D. Middlebrook, “Modelling and analysis of switching DC-to-DC converters in constant-frequency current-programmed mode,” in *IEEE Power Electronics Specialists Conf. Rec.*, 1979, pp. 284–301.
- [14] R.D. Middlebrook, “Topics in multiple-loop regulators and current-mode programming,” in *IEEE Power Electronics Specialists Conf. Rec.*, 1985, pp. 716–732.
- [15] G.C. Verghese, C.A. Bruzos, and K.N. Mahabir, “Averaged and sampled-data models for current mode control: a re-examination,” in *IEEE Power Electronics Specialists Conf. Rec.*, 1989, pp. 484–491.
- [16] R.B. Ridley, “A new, continuous-time model for current-mode control,” *IEEE Transactions on Power Electronics*, vol. 6, no. 2, pp. 271–280, 1991.
- [17] F.D. Tan and R.D. Middlebrook, “A unified model for current-programmed converters,” *IEEE Transactions on Power Electronics*, vol. 10, no. 4, pp. 397–408, 1995.

- [18] J. Sun and R. Bass, "A new approach to averaged modeling of PWM converters with current-mode control," in *Proceedings of International Conference on Industrial Electronics, Control, and Instrumentation*, 1997.
- [19] F.C.Y. Lee, R.P. Iwens, Yuan Yu, and J.E. Triner, "Generalized computer-aided discrete time-domain modeling and analysis of DC-DC converters," *IEEE Transactions on Industrial Electronics and Control Instrumentation*, vol. IECI-26, no. 2, pp. 58–69, 1979.
- [20] G.C. Verghese, M. Elbuluk, and J.G. Kassakian, "A general approach to sample-data modeling for power electronic circuits," *IEEE Transactions on Power Electronics*, vol. 1, no. 2, pp. 76–89, 1986.
- [21] R. Lutz and M. Grotzbach, "Straightforward discrete modelling for power converter systems," in *IEEE Power Electronics Specialists Conf. Rec.*, 1986, pp. 761–770.
- [22] S. Pavljasevic and D. Maksimovic, "Subharmonic oscillations in converters with current-mode programming under large parameter variations," in *IEEE Power Electronics Specialists Conf. Rec.*, 1997, pp. 1323–1329.
- [23] C.-C. Fang, *Sampled-Data Analysis and Control of DC-DC Switching Converters*, Ph.D. thesis, University of Maryland, College Park, 1997.
- [24] H.K. Khalil, *Nonlinear Systems*, Macmillan, New York, 1992.
- [25] A.V. Oppenheim and R.W. Schaffer, *Discrete-Time Signal Processing*, Prentice-Hall, Englewood Cliffs, NJ, 1989.
- [26] I. Zafrany and S. Ben-Yaakov, "A chaos model of subharmonic oscillations in current mode PWM boost converters," in *IEEE Power Electronics Specialists Conf. Rec.*, 1995, pp. 1111–1117.